Gelatin methacrylate hydrogel with drug-loaded polymer microspheres as a new bioink for 3D bioprinting

Adam Mirek, Habib Belaid, Aleksandra Bartkowiak, Fanny Barranger, Fanny Salmeron, Marilyn Kajdan, Marcin Grzeczkowicz, Vincent Cavaillès, Dorota Lewińska, Mikhael Bechelany

Gelatin methacrylate hydrogel with drug-loaded polymer microspheres as a new bioink for 3D bioprinting

Adam Mirek[1, 2], Habib Belaid[2], Aleksandra Bartkowiak[1], Fanny Barranger[2], Fanny Salmeron[3], Marilyn Kajdan[3], Marcin Grzeczkowicz[1], Vincent Cavaillès[3], Dorota Lewińska[1], Mikhael Bechelany[2,4]*

[1] Nalecz Institute of Biocybernetics and Biomedical Engineering, Polish Academy of Sciences, 02-109 Warsaw, Poland

[2] Institut Européen des Membranes, IEM, UMR 5635, Univ Montpellier, CNRS, ENSCM Place Eugène Bataillon, 34095 Montpellier cedex 5, France

[3] IRCM, Institut de Recherche en Cancérologie de Montpellier, INSERM U1194, Université Montpellier, Montpellier F-34298, France

[4] Gulf University for Science and Technology, GUST, Kuwait

Corresponding author: Mikhael.bechelany@umontpellier.fr

GRAPHICAL ABSTRACT

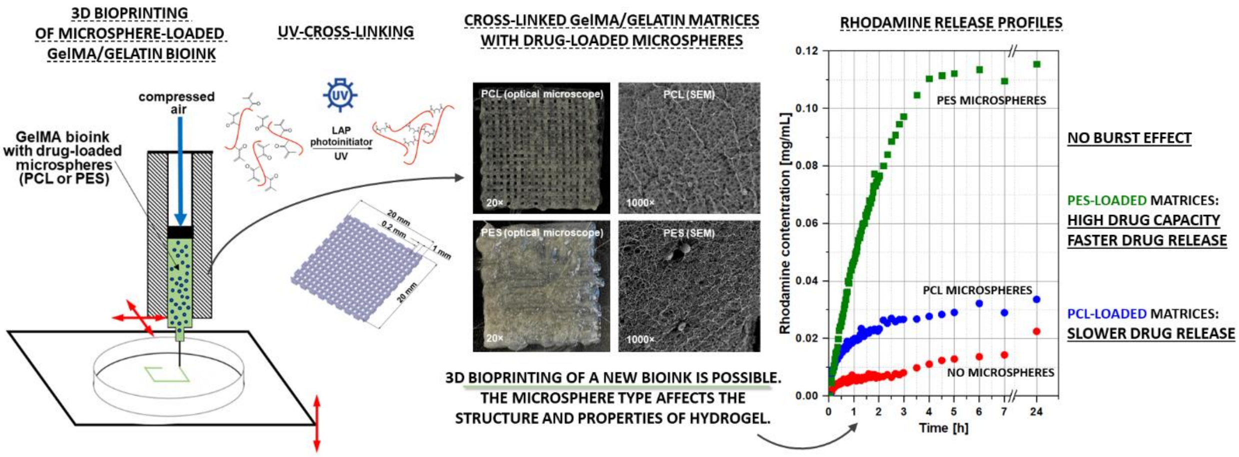

ABSTRACT

3D bioprinted hydrogel constructs are advanced systems of a great drug delivery application potential. One of the bioinks that has recently gained a lot of attention is gelatin methacrylate (GelMA) hydrogel exhibiting specific properties, including UV cross-linking possibility. The present study aimed to develop a new bioink composed of GelMA and gelatin modified by addition of polymer (polycaprolactone or polyethersulphone) microspheres serving as bioactive substance carriers. The prepared microspheres suspension in GelMA/gelatin bioink was successfully bioprinted and subjected to various tests, which showed that the addition of microspheres and their type affects the physicochemical properties of the printouts. The hydrogel stability and structure was examined using scanning electron and optical microscopy, its thermal properties with differential scanning calorimetry and thermogravimetric analysis and its biocompatibility on HaCaT cells using viability assay and electron microscopy. Analyses also included tests of hydrogel equilibrium swelling ratio and release of marker substance. Subsequently, the matrices were loaded with ampicillin and the antibiotic release was validated by monitoring the antibacterial activity on *Staphylococcus aureus* and *Escherichia coli*. It was concluded that GelMA/gelatin bioink is a good and satisfying material for potential medical use. Depending on the polymer used, the addition of microspheres improves its structure, thermal and drug delivery properties.

KEYWORDS

3D bioprinting, bioink, microspheres, drug delivery, gelatin methacrylate, cross-linking

HIGHLIGHTS

- Gelatin methacrylate (GelMA) modified with polycaprolactone (PCL) or polyethersulfone (PES) microspheres as a new useful bioink in 3D bioprinting.
- The type of microspheres used affects the swelling, thermal and transport properties of the 3D bioprinted matrices.
- The microsphere-loaded 3D bioprinted matrices may find potential applications as controlled drug delivery systems or wound dressings.

INTRODUCTION

3D bioprinting involves a variety of advanced manufacturing technologies to produce functional 3D tissues and organs layer by layer using bioink, which includes biological materials, additives and living cells [1]–[3]. Currently, 3D bioprinting technology, is widely used in the design and manufacture of drug delivery systems for therapeutic applications [4]–[6], tissue engineering and regenerative medicine to develop complex tissue structures that mimic native organs and tissues [7]–[10]. The advantages of using 3D bioprinting in the biomedical field are the development of patient-specific personalized designs, high precision and on-demand creation of complex structures in a short time [3].

As mentioned above, bioinks are the materials used in the preparation of processed (bioartificial) living tissues using 3D bioprinting technology. They can comprise only cells, but an extra carrier substance (a biocompatible synthetic or a natural polymer gel or a gel based on the combination of both), which surrounds the cells and acts as a 3D molecular scaffold, is often included. The bioinks used in 3D bioprinting technology should primarily be highly biocompatible and nontoxic, mechanically stable after printing, and should provide high resolution during printing, as well as printing temperatures below physiological temperatures [11]–[13]. Commonly used materials for 3D printing are: polymers, elastomers, ceramics and hydrogels. The most widely used synthetic polymers include: polycaprolactone (PCL), pluronic, polyvinylpyrrolidone (PVP) and polyethylene glycol (PEG). In turn, the most commonly used natural polymers are: gelatin, hyaluronic acid, collagen and matrigel [14].

Gelatin is a natural water soluble protein that comes from the partial hydrolysis of collagen. With its chemical structure and biological functions, it resembles collagen in the native extracellular matrix (ECM). For this reason, it is considered an ideal material that can mimic the natural structure of the ECM. Gelatin is a biocompatible: non-toxic and non-immunogenic polymer and a biomimetic peptide with the ability to prevent cell apoptosis [15]. In addition, gelatin promotes cell proliferation and differentiation in a specific direction [16]. Among other things, these features and the adaptability of gelatin's rheological properties have determined its high popularity as a bioink for use in 3D bioprinting [17], [18].

On the other hand, among the undoubted disadvantages of gelatin that pose an obstacle to the development of bioplastics for medical applications are its poor mechanical and thermal properties. For this reason, in order to obtain a material for use in tissue engineering, among other applications, gelatin is modified with methacrylic anhydride. Recently, gelatin methacrylate (GelMA)-based hydrogels have been widely used in tissue engineering [19]. Other applications of GelMA hydrogels include fundamental cell research, cell signaling, drug and gene delivery, and biosensing [18], [20].

An interesting direction for modifying the properties of newly developed bioinks can be, for example, the addition of microspheres. Microspheres are spherical microparticles with diameters in the range of 1 – 1000 μm that can be loaded with hydrophilic and hydrophobic drugs or other bioactive components (e.g. DNA or proteins). They are usually made from biodegradable and biocompatible polymers, such as: cellulose, polyethersulfone, polycaprolactone, poly(lactic acid) and poly(glucolic acid). Drug release from microspheres occurs by degradation/erosion of the polymer matrix and simultaneous diffusion of the drug substance. Administration of medication via microparticulate systems is advantageous because microspheres can be tailored for desired release profiles and used for site-specific delivery of drugs and in some cases can even provide organ-targeted release [21], [22].

A lot of attention is currently being paid to the development of new bioinks with improved performance properties and for increasingly broader applications, including drug delivery systems and tissue engineering. Our previous work [23] involved an attempt to develop a new bioink based on cross-linked gelatin-alginate hydrogel for potential use as an antibiotic delivery system. Over the past few years, there have been several papers proposing new microsphere-modified bioinks for use in 3D bioprinting [24]–[36]. Mirani et al. [29] used an alginate-gelatin methacryloyl (GelMA)-photoinitiator (PI) solution with suspended *all-trans retinoic acid (ATRA)*-loaded microspheres as the 3D bioprinting material. Three-dimensional porous hydrogel meshes loaded with ATRA-loaded polymer microspheres have been shown to be responsible for, among other things, prolonged ATRA release and induce apoptotic cell death in U-87 MG (malignant glioma). Chen et al. [30] successfully developed bioprinted multiscale composite scaffolds based on gelatin methacryloyl (GelMA)/chitosan microspheres as a modular bioink that mimicked the 3D integrated micro- and macroenvironment of the native nerve tissue very well. Among other things, the effect of these microspheres was shown to increase neurite growth and elongate PC12 cells. Sharma et al. in [31] presented the possibility of using guggulsterone-releasing microspheres contained in a new fibrin-based bioink to bioprint 3D tissues similar to those in the brain. Studies have shown that the addition of drug releasing microspheres to bioink improves cell survival and differentiation. In a subsequent study, Sharma et al. showed that the incorporation of microspheres in bioink enhanced the mechanical strength, lowered the degradation rate, and increased the elastic modulus of bioprinted [32]. In a recent paper [34], Kanungo et al. presented research on an attempt to develop a bioink composed of pectin and Pluronic® F-127 containing gelatin-coated pectin microspheres as vascularization-promoting agents for potential use in tissue bioengineering. When incorporated into bioink for scaffolding, the microspheres distributed evenly and did not display any negative effects on bioprintability. In addition Bonany et al. [36] introduced three types of microspheres with different mineral contents (gelatin, hydroxyapatite nanoparticle- containing gelatin; and calcium-deficient hydroxyapatite) into an alginate-based bioink. The results showed that the addition of microspheres generally improved the rheological properties of the ink, favored cell proliferation and positively affected osteogenic cell differentiation.

So far, the research presented in the literature is primarily concerned with attempts to develop special bioinks modified with drug-loaded microspheres, which act as microreservoirs with internal release of bioactive molecules which improve the survival and differentiation of living cells suspended in the bioink. Such bioinks are designed primarily for 3D bioprinting of tissue scaffolds. However, there is an acute shortage of research on the development of bioinks containing microspheres (microcarriers) to 3D bioprint constructs with external drug release – this kind of bioprintouts can be used as drug delivery systems or dressings for hard-to-heal wounds. In accordance with the assumptions of the presented research, placing microspheres in the 3D bioprinted matrices can guarantee a lot of benefits as follows: prolonged and controlled release of the immobilized substance, increased drug capacity of the entire system, elimination of burst effect and the direct action of drug in the diseased area. For these reasons, an attempt to develop such a bioink was the aim of this work.

The focus was on developing GelMA-gelatin-based bioink modified with two different types of microspheres made of polycaprolactone (PCL) or polyethersulfone (PES) for potential use in 3D bioprinting. These two types of microspheres were prepared as described in detail in our previous work [37]. The properties of the gelatin methacrylate-based bioink were enhanced by the addition of pure gelatin to combine the benefits of both substances. The studies of the printability of bioinks containing GelMA and gelatin in different ratios was conducted by Yin et al. [38], indicating such concentrations of ingredients in which smooth and uniform filaments were formed during bioprinting. The addition of gelatin increases the viscosity and stability of the bioink, as well as the flexibility of the 3D bioprinted model.

Presented research included evaluating the 3D bioprinting feasibility of a newly developed bioink modified with microspheres using an extrusion technique, characterizing the morphology of such 3D bioprinted matrices, assessing their thermal properties and degree of swelling, and evaluating their transport and antibacterial properties.

MATERIALS AND METHODS

Materials

Gelatin type B (CAS Number: 9000-70-8) from bovine skin (gel strength 225 g Bloom), methacrylic anhydride (CAS Number: 760-93-0, ≥94%) sodium chloride (NaCl, CAS Number: 7647-14-5, ≥99%), potassium chloride (KCl, CAS Number: 7447-40-7, ≥99%), potassium phosphate monobasic (KH_2PO_4, CAS Number: 7778-77-0, ≥99%), sodium phosphate dibasic (Na_2HPO_4, CAS Number: 7558-79-4, ≥99) and agar (CAS Number: 9002-18-0) were purchased from Sigma-Aldrich. Polycaprolactone (PCL, M_w = 70 kDa, CAS Number: 24980–41–4) was purchased from Scientific Polymer Products (USA) and polyethersulfone (PES, M_w = 42 kDa, Ultrason E2020) from BASF (Germany). Dimethylformamide (DMF, Chempur, Poland, CAS Number: 68–12–2, ≥99%) and N-methyl-2-pyrrolidone (NMP, Chempur, Poland, CAS Number: 872–50–4, ≥98%) were used as solvents for the polymers (PCL and PES respectively). Ethanol (EtOH, Polmos, Poland, ≥95%) was used as a PCL/PES non-solvent to induce phase separation in a precipitation bath. Lithium phenyl-2,4,6-trimethylbenzoylphosphinate (LAP, Allevi, USA, CAS Number: 85073-19-4, ≥95%) was used as a hydrogel UV-cross-linking photoinitiator. A drug marker rhodamine 640 perchlorate (M_w = 591.05 Da, CAS Number: 72102–91–1) was purchased from Exciton (USA). Ampicillin sodium salt antibiotic (CAS Number: 69–52–3) was obtained from A&A Biotechnology (Poland). The non-pathogenic Gram positive *Staphylococcus aureus* and Gram negative *Escherichia coli* bacteria (K12 DSM 423, from DSMZ, Germany) were chosen as model microorganisms. The culture medium was a Tryptone Salt Broth (TSB, Sigma Aldrich). The chemicals were used without further purification. All solutions were prepared with MilliQ water (with a resistivity of 18.2 MΩ·cm; Millipore, USA).

Gelatin methacrylate synthesis

Gelatin methacrylate (GelMA) was prepared using a protocol first reported by Van Den Bulcke et al. [39] by reaction of gelatin with methacrylic anhydride (MA). In this reaction, the hydroxyl and amine groups of the amino acid residues are substituted with methacryloyl groups (Figure 1A). A constant pH is important to maintain the reactivity of protein functional groups. Gelatin (5 g) was dissolved in phosphate buffer (PBS, pH = 7.4) at 50°C. After 1h MA (5 mL) was added gradually (0.5 mL/min) to the vigorously stirred solution. The reaction was run for at 50°C and after 3 h it was quenched with 250 mL PBS (20°C). The diluted reaction mixture was then dialyzed against deionized water through a dialysis tubing (12 – 14 kDa cutoff) for 7 days to remove potentially cytotoxic low-molecular-weight residues of MA. Dialysis water was changed every 24 hours. The resulting solution was then freeze-dried (48 h at 12 Pa, -70°C) leading to a white solid product – GelMA – which could be stored in a freezer.

Microsphere formation

A technology, the diagram of which is shown in Figure 1C, combining pulsed voltage electrospray with wet phase inversion was used to prepare microspheres [37]. In this process developed in our group, the polymer solution is pumped through a metal nozzle attached to a high pulsed voltage. Microdroplets are created by the electrospray process at the nozzle outlet. Afterwards, they are collected in a well-agitated precipitation bath containing a polymer non-solvent. Based on the Gibbs phase rule, wet phase inversion occurs in this bath, resulting in the formation of hardened polymer microspheres. The procedure can be changed by incorporating different materials (such as drugs) into the polymer solution or bath to immobilize them inside the microspheres. The microspheres were prepared with a 15% solution of PCL in DMF as well as a 15% solution of PES in NMP. The electrical parameters in the study were set to the following values: electrical voltage $U = 8$ kV, pulse frequency $f = 60$ Hz, and pulse duration $\tau = 6$ ms and the polymer solution flow rate was 1.5 mL/h. Throughout the procedure, the temperature did not exceed 25°C and the humidity was not greater than 40%. Microspheres with immobilized active substance were prepared from a polymer solution containing 0.57 mg/g (mass/polymer mass marker) of rhodamine or ampicillin and using a precipitation bath containing 0.1 mg/mL of the substance. Following microsphere formation, the bath suspension was transferred to a falcon and centrifuged to remove the excess ethanol. Then the microspheres were dried, weighed and suspended in distilled water for further use in the bioink preparation. The obtained microspheres had average diameters of 14.38 ± 6.28 µm for PCL and 6.20 ± 2.43 µm for PES.

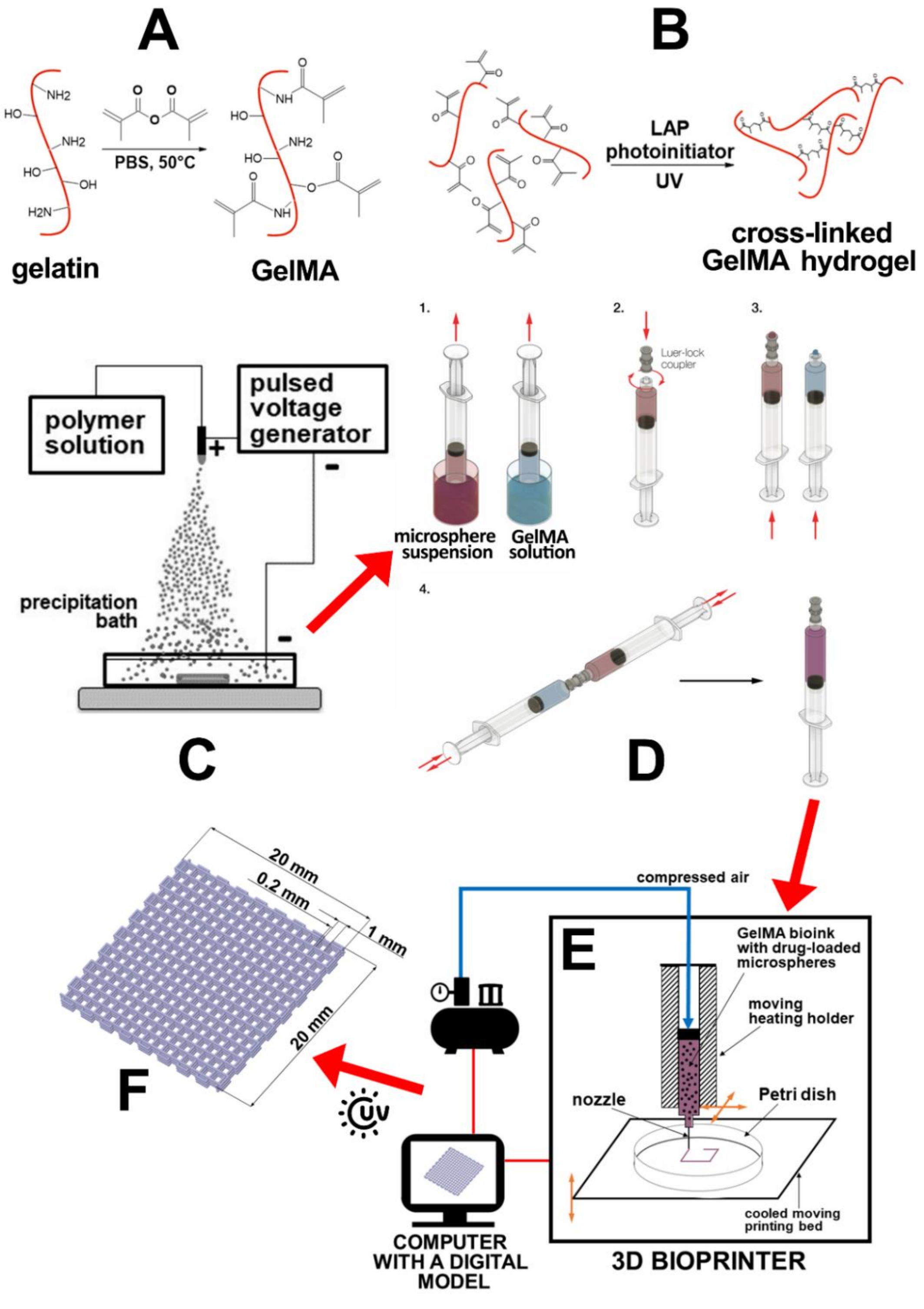

Figure 1. Bioink preparation, 3D bioprinting and UV-cross-linking of microsphere-loaded GelMA/gelatin matrices. (A) Reaction of gelatin and methacrylic anhydride for gelatin methacrylate production. Protein chains are schematically marked with a red line, only amine and hydroxyl groups and their substitutions with methacryloyl groups are shown. (B) Simplified exemplary scheme of reactions during the UV-cross-linking of GelMA to form hydrogel networks – the free radical chain polymerization of the methacryloyl substitutions. (C) The microsphere production process scheme using the method combining electrospray and phase inversion developed previously by the authors [37]. (D) The syringe coupler method scheme proposed by Allevi, Inc. [40] (image used with permission from Allevi) for bioink preparation. Scheme presents mixing microspheres suspension with GelMA solution. (E) 3D bioprinting setup scheme. (F) A digital 3D mesh matrix model designed made using the DesignSpark Mechanical 4.0 software.

Bioink preparation

The bioink presented in this work should be prepared just before it is used in the 3D bioprinting process. For this purpose, three preliminary mixtures were prepared and then combined into the final formulation. Mixture A was a solution of gelatin (10.8 g) in PBS (20 mL) – after 3 hours of stirring at 40°C a 35% solution was obtained. Mixture B was a solution of GelMA (1.19 g) in PBS (7.31 mL) with the addition of LAP (50 mg). A photoinitiator was added to the PBS, stirred for 30 min at 60°C, then GelMA was added and after stirring for 60 min at 60°C a solution containing 14% GelMA and 0.7% LAP was obtained. Mixture C was a suspension of microspheres (PCL or PES, with or without bioactive ingredient) in PBS (or 0.1 mg/mL bioactive ingredient solution in PBS). Appropriate amount of microspheres was suspended in 2 mL of PBS resulting in formation of a suspension of desired microsphere concentration (e.g. 30 mg to get 5 mg/mL bioink suspension in the next step). Once all mixtures were ready, the syringe coupler method (Figure 1D) was used to prepare the suspension for 3D bioprinting. A similar methodology was employed by Jeon et al., as evidenced in their work [41]. The mixtures were transferred to syringes: 1.9 mL of mixture A, 2.1 mL of mixture B and 2 mL of mixture C. First, the syringes A and C were linked with a syringe coupler, and the contents were mixed by moving the plungers back and forth 40 – 50 times. The resulting suspension of microspheres in gelatin solution was then placed in one of the syringes which was connected with a syringe coupler to the third syringe containing the mixture B. Again, the plungers were moved back and forth 40 – 50 times. In this manner, a suspension of microspheres with concentrations 5 mg/mL or 10 mg/mL in a 11% gelatin and 5% GelMA solution in PBS with a 0.25% addition of LAP was obtained.

3D bioprinting of GelMA/gelatin matrices

Once the bioink was ready, it was set in the heating holder of bioprinter (Figure 1E) and then 3D model could be printed (Figure 1F) forming hydrogel matrices cross-linked using UV light.

As a digital model of a bioprinting matrix, a cubic mesh (the grid size was set as 1 mm and line width as 0.2 mm) with dimensions of 20 mm × 20 mm × 12 mm made of 6 layers (0.2 mm in height each) was designed (Figure 1F). The 3D model project was made in the DesignSpark Mechanical 4.0 software, exported as an STL file, sliced by Repetier-Host/Slic3r software and converted into G-code. The microsphere-loaded GelMA/gelatin matrices were printed using Allevi 2 3D bioprinter (Philadelphia, USA). Figure 1E presents the scheme of the experimental setup. Bioprinting parameters were set as follows: temperature of the bioink in the syringe of

28°C, temperature of the collector Petri dish of ~15°C, printing pressure of 345 kPa (50 psi), printing speed of 10 mm/s, G30 nozzle (inner diameter of 0.164 mm), layer height of 0.2 mm.

The cross-linking of the bioprintout from the GelMA/gelatin bioink was carried out in two stages: first, the gelatin was thermally cross-linked directly on the collector, hydrogen bonds were formed, and then the initially hardened matrix was exposed to UV light, initiating GelMA cross-linking. During UV-curing of the GelMA/gelatin hydrogel in the presence of LAP, free radicals are generated from the photoinitiator. They initiate chain polymerization of methacryloyl substitutions and propagation between methacryloyl groups located on the same or different chains takes place (Figure 1B). In the described research, samples of a freshly printed hydrogel matrix were placed in a chamber emitting ultraviolet light with a wavelength of 365 nm in a vertical position so that the entire sample was evenly illuminated. Two lengths of cross-linking time were tested: 5 min and 10 min.

Ten types of samples (without immobilized bioactive substance) differing in the content of microspheres in the bioink and cross-linking time were prepared in the manner described above. The obtained GelMA/gelatin matrices are summarized in Table 1. with a proper denotation for each of them (the first number corresponds to the microsphere content in the bioink, the second number – to the UV-cross-linking time expressed in minutes).

Table 1. List of bioprinted GelMA/gelatin matrices differing in microsphere content and cross-linking time.

Sample	**Details**	
0_0	no microspheres	no UV-cross-linking
0_5	no microspheres	5 min of UV-cross-linking
0_10	no microspheres	10 min of UV-cross-linking
5_0_PCL	5 mg/mL PCL microspheres	no UV-cross-linking
10_0_PCL	10 mg/mL PCL microspheres	no UV-cross-linking
5_5_PCL	5 mg/mL PCL microspheres	5 min of UV-cross-linking
5_10_PCL	5 mg/mL PCL microspheres	10 min of UV-cross-linking
5_0_PES	5 mg/mL PES microspheres	no UV-cross-linking
5_5_PES	5 mg/mL PES microspheres	5 min of UV-cross-linking
5_10_PES	5 mg/mL PES microspheres	10 min of UV-cross-linking

In addition, six types of samples for testing the transport properties of bioprinted matrices (microsphere content: 0 mg/mL or 5 mg/mL and cross-linking time 5 or 10 minutes) and four types of samples for testing antibacterial properties (microsphere content: 0 mg/mL or 5 mg/mL and cross-linking time 10 minutes) were prepared. The GelMA/gelatin matrices for studies requiring anhydrous samples were frozen (8 h at -20°C) and lyophilized (24 h at 12 Pa, -70°C).

Characterization of the cross-linked GelMA/gelatin matrices

The 3D bioprinting feasibility with proposed new bioink was assessed on the basis of observations made during the process, as well as based on printouts examined using digital microscope (Keyence, VHX-7000). After that, the samples were lyophilized and observed with scanning electron microscopy (SEM, HITACHI S4800) – the samples were coated with 10 nm thick gold layer for it.

Fourier Transform Infrared Spectroscopy (FTIR) was used to determine which functional groups are present in the analyzed sample and thus the influence of microsphere use as well as crosslinking on it. The FTIR spectra of GelMA/gelatin matrices was recorded using the NEXUS instrument equipped with and attenuated total reflection (ATR) accessory in the frequency range of 500-4000 cm^{-1} with an average of 64 scans at 2 cm^{-1} resolution.

Thermal properties of samples were investigated using differential scanning calorimetry (DSC) and thermogravimetric analysis (TGA). Differential scanning calorimeter (DSC, TA Instruments 2920) equipped with a RCS90 cooling system was used to determine the thermal transition points and enthalpies (calculated as an area under the peak) of the GelMA/gelatin matrices. The samples were weighed (~ 2-3 mg) in an aluminum TA pan and sealed, an empty sealed pan was used as a reference. The samples were cooled to -80°C and then heated up to 200°C with a heating rate of 20°C/min. TA Instruments TGA G500 apparatus was used to perform the thermogravimetric analysis under oxygen flow of 60 mL/min to define the cross-linking influence on a thermal stability of matrices. The samples of ~ 3-12 mg were heated up to 1000°C at a heating rate of 10°C/min.

Samples for FTIR, DSC and TGA were frozen (8 h at -20°C) and lyophilized (24 h at 12 Pa, -70°C) before the analyses.

Cell culture and cytotoxicity assays

HaCaT cells (spontaneously transformed human keratinocytes) were cultured at 37°C in 5% CO_2 using DMEM (Dulbecco's Modified Eagle Medium α) media supplemented with 10% (v/v) foetal bovine serum. HaCat cells (10^4 cells per well) were seeded in 96 well plates and allowed to attach for 24 hours. After sterilization with UV irradiation for 1 hour, the hydrogels were hydrated in culture medium for 24 hours. The corresponding hydrogel eluates (25 mg/ml) was prepared and the culture medium of the HaCaT cells seeded in 96 well plates was replaced by 100 µl of the hydrogel eluate at various dilutions (up to 50-fold). After 24 hours of incubation with the hydrogel eluates, cell viability was analyzed using MTT assay carried out as previously described [23] or with the CyQUANT® Cell Proliferation Assay Kit (Invitrogen, France) with a measurement of fluorescence at 520 nm on a Pherastar fluorimeter. Alternatively, HaCaT cells were also seeded directly onto the hydrated hydrogels (100 µl of cell suspension in 96 wells plate corresponding to 1.5×10^3 cells/well). After 16 hours, the number of viable cells was determined by adding 11 µl of Alamar blue HS Cell Viability Reagent (Thermofisher, France) and fluorescence was measured 1 hour later on a Pherastar fluorimeter (excitation 540 nm/emission 590 nm). Data (n=3 to 18) were analysed statistically using the Student t-test or the Mann-Whitney test.

Scanning electron microscopy analysis of cell-seeded matrices

HaCaT cells (1.2×10^6 cells/well in 12 wells plate) were seeded onto the different hydrogels previously hydrated and washed 3 times in cell culture medium. After 16 hours of culture, the hydrogels were washed with PBS, fixed with 2.5% glutaraldehyde in PHEM buffer (pH 7.2) for 1 hour at room temperature and washed again in PHEM buffer. Fixed samples were dehydrated using a graded ethanol series (30-100%), followed by 10 minutes in graded ethanol/hexamethyldisilazane (HMDS), and then HMDS alone. Subsequently, the samples were sputter coated with a 10 nm thick gold film and then examined under a scanning electron microscope (Hitachi S4000) using a lens detector with an acceleration voltage of 10 kV at calibrated magnifications.

Swelling properties of the cross-linked GelMA/gelatin matrices

3D bioprinted, crosslinked and lyophilized GelMA matrices were cut and weighted. Then, their equilibrium swelling ratio (ESR) in PBS at 37 °C was determined using a gravimetric method. Each sample (~ 60 – 150 mg, W_d) was placed in closed bottle with 10 ml of swelling medium (PBS). After predetermined immersion time intervals, they were retrieved and weighed (Wt) and placed again in PBS (surface water was gently removed with a tissue before measurements). The water ESC at time *t* was calculated according to the following equation:

$$ESR = \frac{W_t}{W_d} \cdot 100\% \qquad (1)$$

where Wt is the sample weight at a particular time (t) and Wd is the weight of dried matrix.

The experiment was performed three times for different samples of each type of GelMA/gelatin matrix were used to perform and average ESR value as calculated.

Model drug molecule (rhodamine) release from the GelMA/gelatin matrices

The release profile of rhodamine 640 from GelMA/gelatin matrices was determined for six types of samples – with marker and no microspheres, with marker-loaded PCL microspheres and with marker-loaded PES microspheres, each group of samples UV-cross-linked for 5 or 10 minutes. Rhodamine 640 was used in the experiments because its concentration in the solution can be easily, quickly and accurately determined spectrophotometrically, which allows the transport properties of the system to be observed (including possible burst effect). A sample of 22.1 – 38.1 mg of each freeze-dried GelMA/gelatin matrix was placed in a glass container with 3.65 – 6.3 mL of deionized water (the amounts were selected so as to maintain a constant proportion between the weight of the sample and the volume of water ~ 1:6). The content of the container was stirred all the time and the total volume did not change during the experiment. A flow spectrophotometric method proposed before by Grzeczkowicz et al. [42] was used for the tests to determine rhodamine concentration (light wavelength of 574 nm used). Measurements of absorbance were made as follows: every 2 minutes for the first 2 hours, every 10 minutes for the next 1 hour, every 30 minutes for the next 2 hours, after 6, 7 and 24 hours. On the basis of the data, the rhodamine release profiles from GelMA/gelatin matrices were plotted on graphs. The transport properties of the tested matrices were described mathematically with a linear function fitted to the plotted experimental points of the initial one hour of the substance release. A line describing each case ($y = ax$) *was* fitted in OriginPro software. The coefficient a defines the slope of the line and thus the substance release rate. In addition, a graph showing the concentration of rhodamine in solution after release in various samples for 24 hours was plotted to check whether (and how) the addition of microspheres increases the amount of rhodamine released from the matrix compared to one without microspheres. The experiments were done three times, the average light absorbance (thus marker concentration) values were calculated.

Antibacterial activity of the GelMA/gelatin matrices with ampicillin-loaded microspheres

For the antibacterial tests four types of GelMA/gelatin matrices were prepared, all UV-cross-linked for 10 minutes – with no ampicillin, with ampicillin (no microspheres), with ampicillin-loaded PCL microspheres and with ampicillin-loaded PES microspheres. The sterilization was provided by the UV cross-linking. *Staphylococcus aureus* (*S. aureus*, Gram positive) and *Escherichia coli* (*E. coli*, Gram negative) bacteria were used to examine the antibacterial activity of the samples. Microbiological agar (15 $g \cdot L^{-1}$) was added to PBS to prepare Mueller-

Hinton agar (GMH) plates. Two rectangular dishes– each for one type of bacteria – were inoculated individually with 1 mL of *S. aureus* or *E. coli* suspension. The optical density at 620 nm (OD600) of the bacterial suspension was then adjusted to 0.75 ± 0.01 for *S. aureus* and 0.80 ± 0.01 for *E. coli*. Immediately after the inoculation, the samples were put onto the dishes to check the ability of the drug-loaded matrices to prevent bacterial growth. The plates were then incubated overnight at 37°C in aerobic conditions so the bacterial biofilm could be formed. The plates were pictured to show inhibited bacterial growth (the clear zones). The study outcomes were measured by quantifying the area of the inhibition zone through three replicates of each test condition, five measurements for each. Average area values were calculated and statistical significance of the measurements was determined using a one-way analysis of variance test (ANOVA) followed by a post-hoc Tukey HSD test. The results were presented in a bar chart, which included the average values and standard deviations, facilitating their comprehension.

RESULTS AND DISCUSSION

3D bioprinting feasibility

The 3D bioprinting is multi-step process, and at each stage certain decisions must be made regarding its conditions affecting the final product – a hydrogel matrix. First, the composition of the bioink should be developed. On the basis of own experimental selection as well as the work of Yin et al. [38], it was decided to conduct research with bioink containing 5% GelMA and 11% gelatin. The bioink was modified by adding PCL or PES microspheres, selecting their content so that it is still printable. Then, a number of experiments were carried out to determine the optimal printing conditions to obtain GelMA/gelatin matrices compatible with the digital model. The obtained bioprintouts were analyzed using digital microscopy to characterize their macrostructure and microsphere distribution. The results in the form of images of matrices differing in the content and type of microspheres and UV-cross-linking time are shown in Figure 2.

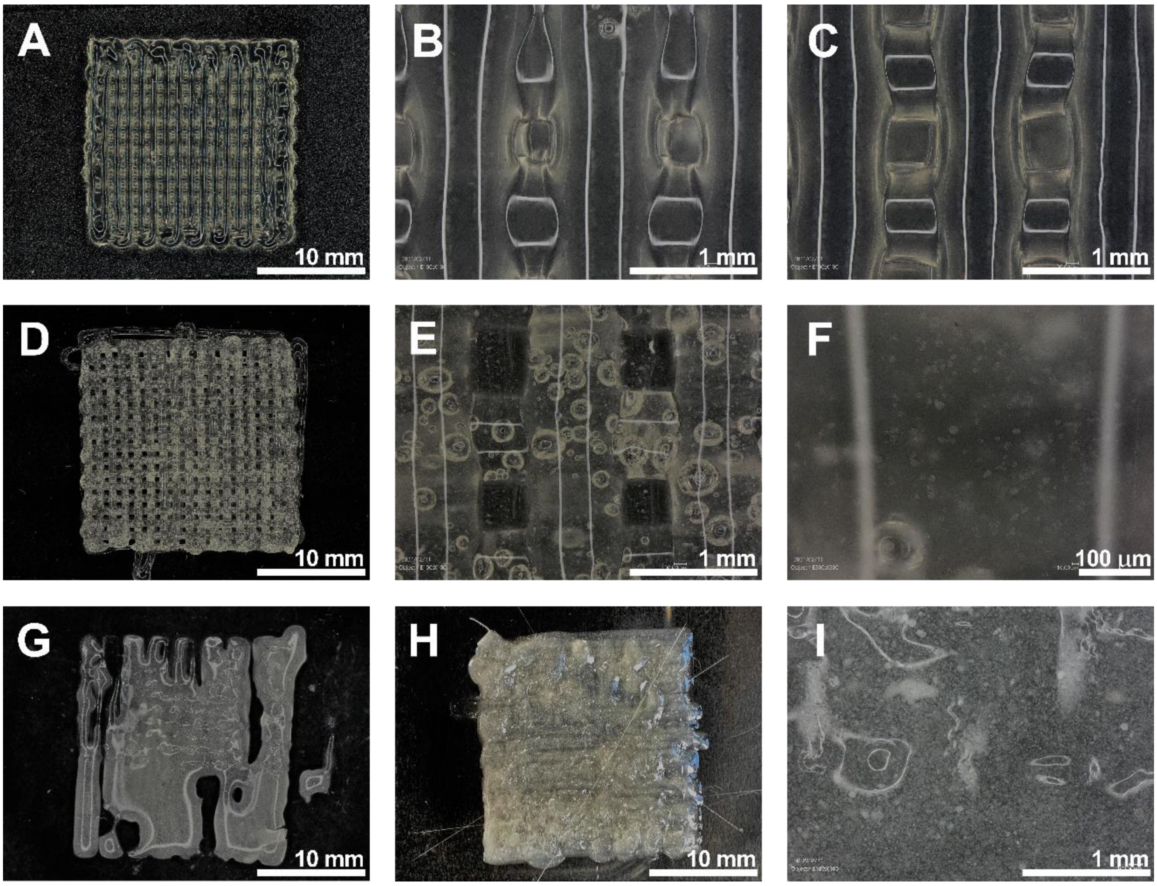

Figure 2. 3D bioprinted GelMA hydrogel (5% GelMA, 11% gelatin) matrices before lyophilization pictures made with digital microscope. (A – B) Bioink without additives, matrix immediately after printing, no cross-linking, magnification (A) 20× and (B) 100×. (C) Bioink without additives, matrix UV-cross-linked for 10 minutes, magnification 200×. (D – F) Bioink with 5 mg/mL PCL microspheres, matrix UV-cross-linked for 10 minutes, magnification (D) 20×, (E) 100×, (F) 500×. (G) Bioink with 10 mg/mL PCL microspheres, unable to bioprint a model matrix, magnification 20×. (H – I) Bioink with 5 mg/mL PES microspheres, matrix UV-cross-linked for 10 minutes, magnification (D) 20×, (E) 100×.

Addition of gelatin to the GelMA bioink eliminated the need for photochemical cross-linking during the bioprinting process (between each subsequent printed layer), which reduced the interruptions in printing caused by clogging of the nozzle with elements of unintentionally cross-linked bioink inside it. The concentrations of ingredients that were chosen provided smooth and uniform filaments formed during 3D bioprinting.

In the case of the non-cross-linked GelMA/gelatin matrix (A), its structure coincides with the matrix designed using the computer model in Figure 1F, but the sizes of the model elements (gaps, grids) are not the same. In the case of gaps, the size decreased (the gap size in the model is 1 mm, in the bioprinted matrix it is 0.3 mm) and for grids it increased (the grid width in the model is 0.2 mm, in the bioprinted matrix it is around 0.7 mm).

In addition, analysis of the images (B and C) suggests that there are no significant changes in the structure of the 3D printed matrix after the UV-cross-linking process. The only observable difference is a slight blurring of the structure of the non-cross-linked matrix (B) – the shrinkage effect of the non-cross-linked matrix is not observed in the cross-linked one.

The content of microspheres in the GelMa/gelatin matrix (5 mg/ml) leads to structures with slightly more "spilled" shapes (D). The obtained images of the macroscopic structure of the matrices also confirm the presence of PCL microspheres with diameters of about 10 – 14 μm evenly distributed in the 3D printed matrix structure (E and F). On the other hand, the content of microspheres in the bioink at the level of 10 mg/ml completely disabled the printing of the constructs (G). It can also be observed that numerous air bubbles were present in the structures of the 3D printed constructs (E) being a result of intense mixing the components with syringe coupler method during bioink preparation. Further bioink development is suggested to elaborate a method to remove the bubbles before printing.

In the case of GelMA/gelatin matrices modified with PES microspheres (H, I), the 3D bioprinting was possible. However, it was not possible to obtain a structure in accordance with the designed one (Fig. 1F). The 3D bioprinting conditions were identical as in the case of matrices without microspheres or with PCL microspheres. The presence of PES microspheres probably affects the rheological properties of the bioink used, which affects the 3D printed matrix. Another reason for obtaining such a 3D printed matrix can be attributed to the different thermal properties of the PES microspheres. Moreover, the fact that the structure is kept or not, is related to the interaction between PCL/PES and GelMA/gelatin. In the case of polycaprolactone (PCL), the intermolecular forces (hydrogen bonding or van der Waals forces) allows the matrix to keep the designed structure during printing enhancing the thermal cross-linking. It has been shown that three potential kinds of inter- and the intramolecular hydrogen bondings can occur in the PCL molecule between the CH2 and C=O groups [43]. In addition, there are also intermolecular dipole–dipole interactions (C=O···C=O) between PCL and GelMA/gelatin molecule [44]. All these interactions are weaker for polyethersulphone (PES) microspheres, because there is only one hydrogen bonding acceptor (–O–) in the polymer structure and no donors, the matrix structure is therefore not preserved. Due to this, the conditions for 3D bioprinting of PES-loaded GelMA/gelatin bioink and its composition should be selected individually. However, it was decided not to change them and use them in further research in order to be able to compare the obtained results without hindrance.

The 3D bioprinting process with GelMA/gelatin microsphere-loaded bioink can be influenced by many factors, the proper selection of which allows it to be carried out and lead to the expected product in the form of a hydrogel matrix. In addition to the already mentioned UV exposure time or the content of microspheres, others can be indicated: the degree of substitution during the reaction of gelatin with MA, bioink composition (gelatin – GelMA ratio), photoinitiator concentration, bioprinting parameters. The major parameters allow tuning of the physical properties of the GelMA hydrogels must be selected experimentally to be matched to the expected results.

Effect of UV-cross-linking and lyophilization on the structure of GelMA/gelatin matrices

The surface morphology, chemical structure and thermal properties of 3D bioprinted GelMA/gelatin matrices was examined using such techniques as SEM, FTIR, DSC and TGA. The samples were dehydrated in this part of research – all of the matrices were lyophilized as described in the Materials and methods section. Scanning electron microscopy pictures of different GelMA/gelatin matrices is presented in Figure 3.

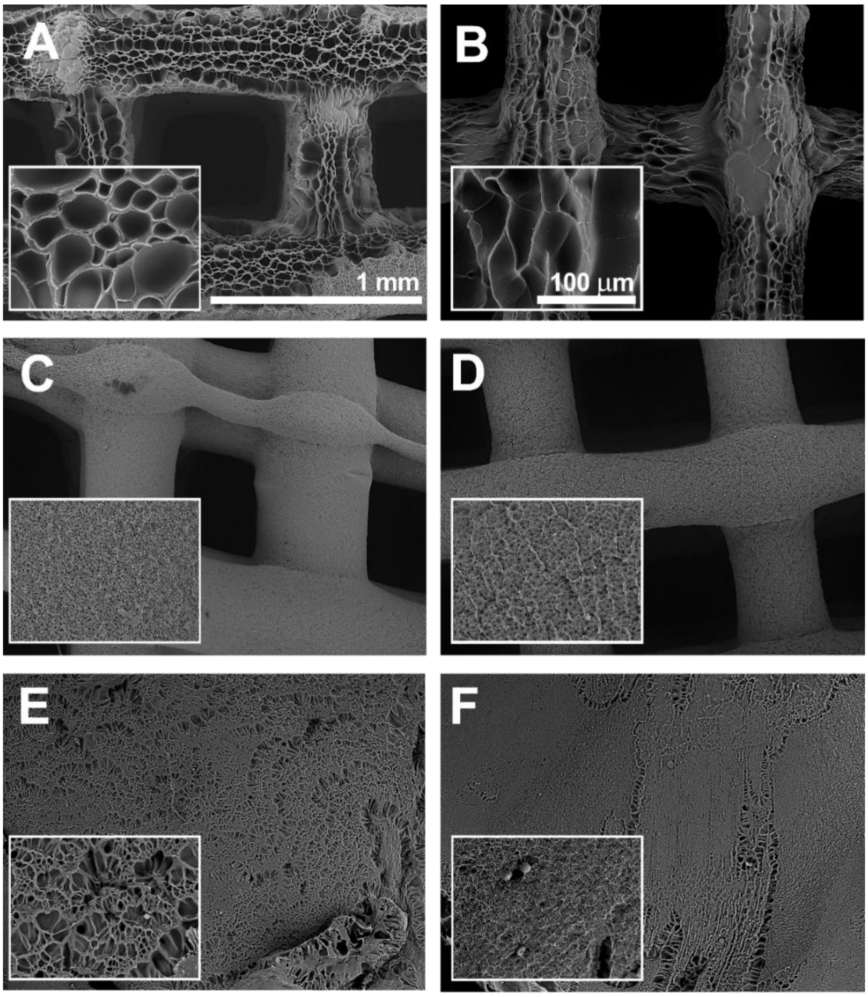

Figure 3. SEM pictures of lyophilized GelMA/gelatin matrices: (A) no microspheres, no UV-cross-linking, (B) no microspheres, 10 minutes of UV-cross-linking, (C) 5 mg/mL PCL microspheres, no UV-cross-linking, (D) 5 mg/mL PCL microspheres, 10 minutes of UV-cross-linking, (E) 5 mg/mL PES microspheres, no UV-cross-linking, (F) 5 mg/mL PES microspheres, 10 minutes of UV-cross-linking – magnification 100×; close-up of surface structures – magnification 1000×.

Based on the scanning electron microscopy (SEM) images (Figure 3), the morphology of lyophilized non-cross-linked (A) and UV-cross-linked (B) GelMA/gelatin matrices, as well as the ones modified with PCL (C, D) and PES (E, F) microspheres was evaluated. Both analyses the one of images obtained by optical microscopy (Figure 2) as well as the one of the SEM images (Figure 3), indicate, first of all, a clear effect of the lyophilization process on the morphology of the GelMA/gelatin matrices studied. Their surfaces after the lyophilization process are highly corrugated and porous/wrinkled. Matrices (A–D) retained the structure of a regular grid after drying with visible layers. There are no significant differences in the morphology of UV-crosslinked and non-UV-crosslinked matrices (without the addition of microspheres) (Figure 3 A and B). In contrast, modification of the 3D printed matrices with PCL microspheres leads to matrices with a significantly more compact and homogeneous structure (Figure 3 C–D). The PCL microspheres probably acted as a filler that prevented the dried surface from creasing strongly, the shrinking hydrogel was retained on the microspheres in this case, in contrast to the matrices without microspheres, whose surface is severely wrinkled. Modification of the bioink with PES microspheres led to the formation of a completely different structure of the GelMA/gelatin matrix than in the other cases, which was already noticed in the analysis of samples by optical microscopy. In this case, the effect of cross-linking on the structure is noticeable – matrices exposed to UV light for 10 minutes are less porous.

Fourier transform infrared spectroscopy (FTIR) was performed to check the effectiveness of dialysis during GelMA synthesis as well as the influence of the addition of microspheres and UV-cross-linking on the chemical structure the GelMA/gelatin matrices. Fig. SI1 (supporting information) presents the results. The IR spectra of non-crosslinked GelMA/gelatin matrix without microspheres (0_0) show all characteristic chemical functional groups – the broad peak at 3291 cm^{-1} is attributed to the O–H and N–H stretching vibrations, two peaks between 2800 – 3100 cm^{-1} denoting C–H stretching of –CH2 and tertiary –CH groups present in both gelatin and methacryloyl functional groups, the backbone structure of gelatin is denoted by peaks at 1635 cm^{-1} (amide I, C=O stretching), 1543 cm^{-1} (amide II, N–H bending), 1236 cm^{-1} (amide III, C–N stretching). There are no strong peaks between 1690 – 1760 cm^{-1}, characteristic for methacrylate anhydride, indicating the carbonyl (C=O) group, which means that the post-reaction residues of this substance have been completely removed from GelMA. There are no peaks typical for microsphere-forming polymers in either spectrum – neither 1750 – 1735 cm^{-1} indicating C=O stretching in carboxylic esters (PCL) nor 1350 – 1300 cm^{-1}

indicating S=O stretching in sulfones (PES). There are also no new chemical bonds between GelMA, gelatin and microspheres. The addition of microspheres does not affect the chemical structure of the hydrogel.

The thermal properties of the UV-cross-linked GelMA/gelatin matrices with microspheres were determined by TGA and DSC (Fig. 4A and B). For reference purposes, an analysis of pure substances was also performed: gelatin, PCL and PES.

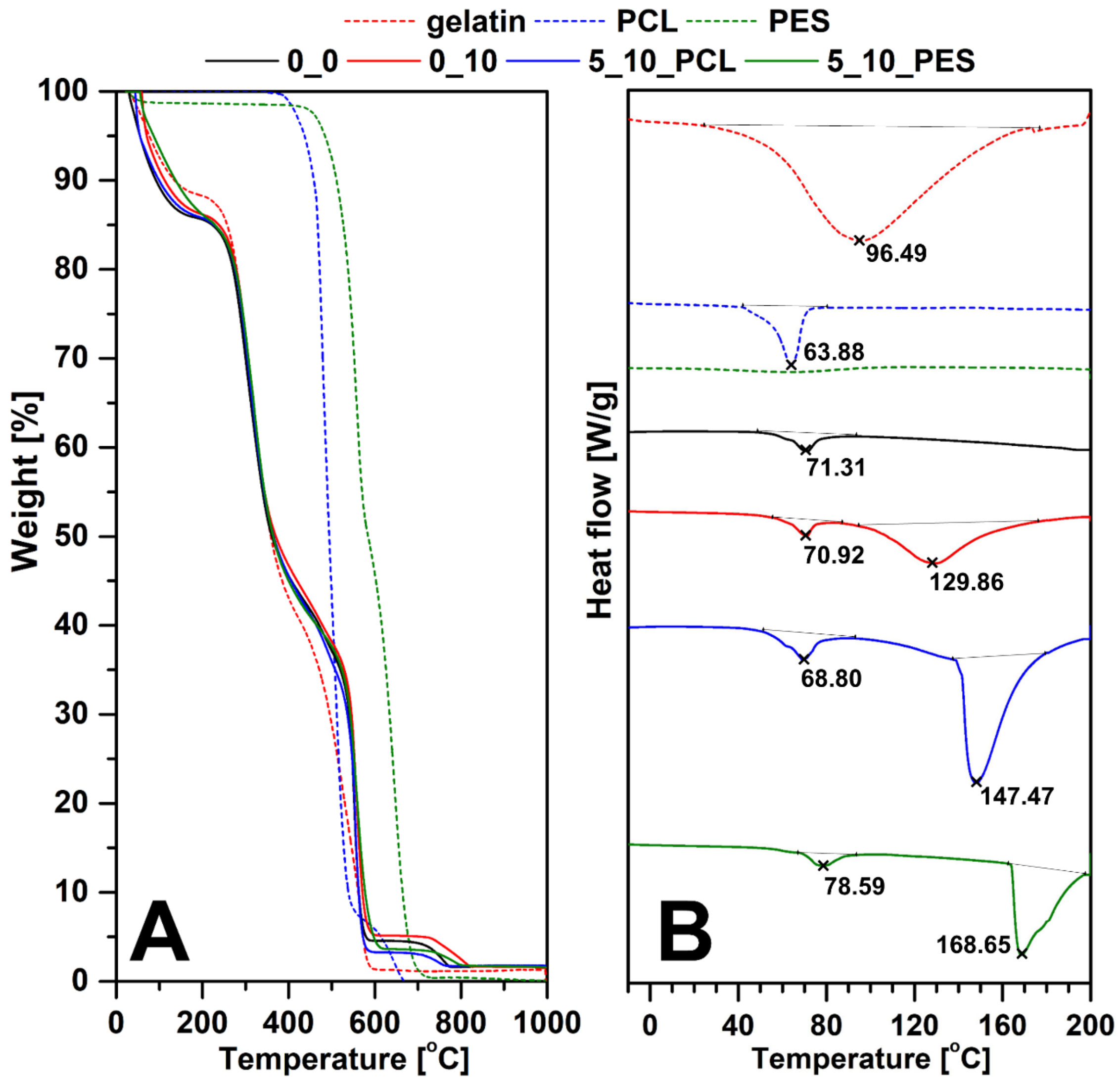

Figure 4. Thermal properties of GelMA/gelatin matrices. Four samples were analyzed in each case: non-cross-linked matrix without microspheres (black) and 10 minutes cross-linked matrices without microspheres (red), with PCL (blue) or PES (green) microspheres. (A) Thermogravimetric analysis and (B) differential scanning calorimetry of pure gelatin, PCL and PES as well as GelMA/gelatin matrices.

Table 2. Thermal transition enthalpies (ΔH_1 – melting or helix-coil transition, ΔH_2 – melting) with the total enthalpy change ΔH for pure gelatin, pure PCL, pure PES and four types of lyophilized 3D bioprinted GelMA/gelatin matrices.

Sample	ΔH_1 [J/g]	ΔH_2 [J/g]	ΔH [J/g]
Gel powder	294.3 ± 8.8	-	294.3 ± 8.8
PCL polymer	32.0 ± 2.1	-	32.0 ± 2.1
PES polymer	8.0 ± 0.2	-	8.0 ± 0.2
0_0	11.8 ± 0.3	-	11.8 ± 0.3
0_10	7.7 ± 0.2	55.2 ± 3.1	62.872 ± 3.3
5_10_PCL	17.0 ± 1.1	195.2 ± 5.4	212.23 ± 6.5
5_10_PES	13.3 ± 0.8	46.5 ± 2.4	59.76 ± 3.2

According to TGA (Fig. 4A), the first weight loss of pure gelatin (approx. 12-15%) occurs in the temperature range 30°C – 160°C and is attributed to the decrease in the content of structural water (bound to protein molecules by hydrogen bonds) and various volatile impurities. The largest weight loss in the range of 220°C – 600°C by about 86% results from the degradation of gelatin molecules. PCL shows only one weight loss (100%) related to the decomposition of the polymer chain from about 360°C to 675°C. For PES it is similar, one total weight loss over the temperature range of 420°C to 730°C. In the case of bioprinted matrices made of bioink containing GelMA and gelatin, there are three stages of mass loss in each case, and all four thermogravimetric curves have similar shapes, they are only slightly shifted relative to each other. The non-cross-linked GelMA/gelatin matrix without microspheres (0_0) loses mass for the first time in the temperature range of 30°C – 190°C (15% loss), i.e. at a temperature such as pure gelatin, it is analogously related to the loss of structural water. For 10 minute UV-cross-linked samples (0_10, 5_10_PCL and 5_10_PES), the first weight loss (15% loss) starts at a higher temperature (around 50°C) because it is more difficult to remove water from the highly UV-cross-linked polymer network. The second stage of weight loss is also shifted in relation to pure gelatin, especially in terms of the decrease from 50% to 5% of weight – for hydrogel samples it occurs in the temperature range of 360°C – 600°C and is less mild. It results from GelMA content in bioink as well as the cross-linking, which causes the degradation of the polymer to occur at a higher temperature. The second stage of weight loss ends in the case of hydrogel at about 3 – 5% mass, which is higher than for pure gelatin, confirms the presence of gelatin methacrylate in the sample. The third stage of mass loss does not occur in the case of pure gelatin, and for the hydrogel it runs in the range of 725°C – 825°C and results from the degradation of GelMA. At the end of the analysis, all tested samples and pure gelatin show about 1.5% residue. The content of microspheres in bioink is so small in relation to gelatin and GelMA (about 30 times less) that their percentage in the TGA chart is negligible. The assessed thermal stability of the dried GelMA/gelatin matrices suggests that they do not degrade at temperatures below 121°C, which is particularly important for biomedical devices and products that are subjected to autoclaving sterilization at this temperature.

In DSC research pure gelatin showed wide endothermic peak in the temperature range of 25 – 170°C, with endothermic enthalpy change of 294.3 J/g, which represents changes in the structure of polymer chains and the dehydration [45]. The DSC diagram corresponding to the PCL that it exhibits one endothermic peak (around 64°C), which determines its melting point [46], while the curve for PES does not show any peak – it would appear at the melting point of the polymer (around 230°C) [47], but it is outside the tested range important from the point of view of the biomedical hydrogel.

There are two endothermic peaks observed for each of GelMA/gelatin hydrogel samples. There is no peak corresponding to the melting enthalpy of ice at 0°C, suggesting that the lyophilization of the samples was successful and no free or freezable water was left in the matrices [48]. The diagrams also do not exhibit any peak that would correspond to the phase transition of the hydrogel due to the presence of nonfreezable water in it. Such a peak was observed by Mirek et al. [23] for gelatin-alginate hydrogel at about 37°C and by Yoshida et al. [49] for hyaluronic acid, xanthan and pullulan hydrogels – the lack of non-freezable water in GelMA/gelatin hydrogel results from the lack of polysaccharides in the bioink. This beneficial phenomenon prevents changes in the structure of dried matrices at elevated temperature.

The first peak appearing in the DSC diagrams can be attributed to the release of bound water and the helix-coil transition of gelatin in the range of around 45 – 85°C. At low temperatures, gelatin exhibits a high triple-helix level that decreases upon heating forming a random coil structure. Such a shift of the transition start towards higher temperatures in relation to pure gelatin (from 25°C to 45°C) results from the high content of GelMA in the sample. In GelMA, the triple-helix level is initially much lower than in the gelatin structure – intrachain hydrogen bonds in the gelatin's triple helix are reduces due to methacryloyation of free amino groups or hydroxyl groups, which leads to random coil level increase (helix level decrease) [39]. The enthalpy of the process is lower than for pure gelatin (7.7 – 17.0 J/g) due to the lower triple-helix level in GelMA/gelatin matrices. It is the highest for samples containing PCL microspheres (17.0 J/g), because of two overlapping effects – gelatin helix-coil transition and polymer phase transition (around 64°C).

The second endothermic peak appears for the UV-cross-linked hydrogel samples and is related to the degradation of the material. This process is definitely more difficult in the case of a hydrogel which in its structure contains intrachains connected by methacrylic anhydride functional groups which reduces chain mobility [50]. In the case of GelMA/gelatin matrix without microspheres, the peak corresponding to the enthalpy of degradation (55.2 ± 3.1 J/g) ranges from 87°C to 180°C. The peak narrows and shifts towards higher temperatures (140°C – 190°C for PCL, 160°C – 195°C for PES), when polymer microspheres are added to the hydrogel, the process enthalpy increases significantly (195.2 ± 5.4 J/g) when PCL microspheres are used.

Differences in the thermal properties of the tested materials (ΔH change and different temperature values) could be related to several factors as follows: chemical interaction between polymers, homogeneity of microsphere dispersion, fraction of each polymer resulting from its obtaining method, porosity of microspheres, bioprintout structure, degree of cross-linking, etc. The explanation of the reasons for their properties requires further research. However, shift of the degradation temperature of bioprinted matrices towards higher values after adding microspheres to bioink is a beneficial effect from the point of view of the potential use of the proposed hydrogel for biomedical purposes due to the previously mentioned autoclaving temperature.

Biocompatibility of GelMA hydrogels with human keratinocytes

Using human keratinocytes (HaCat cells), the cytocompatibility of the 3D bioprinted gelatin-methacrylate hydrogel matrices was evaluated in order to validate their potential future use as wound dressings. The biocompatibility of the GelMA hydrogels (containing or not PCL or PES microspheres at a concentration of 5 mg/ml) was analyzed in an indirect contact test.

As shown in Figure 5A, after 24 hours of culture, a slight cytotoxicity was observed with the different hydrogel eluates at the highest concentrations (10 and 25 mg/ml), when tested using the MTT assay. At these concentrations, the GelMA hydrogels containing PCL or PES microspheres where significantly more cytocompatible than the control hydrogel without microspheres. No significant differences in cytocompatibility were observed between the three hydrogels when tested using the Cyquant dye, which relies on the direct measurement of fluorescence following its incorporation into DNA (Figure 5B). These data suggest that the matrices were not cytotoxic in the experimental conditions tested. The proliferation of HaCaT cells in the presence of hydrogel eluates was also monitored and, as shown in Figure 5C, a slight (around 2-fold) reduction of cell proliferation as compared to control cells grown in the culture medium was observed and again, the three hydrogels behaved similarly.

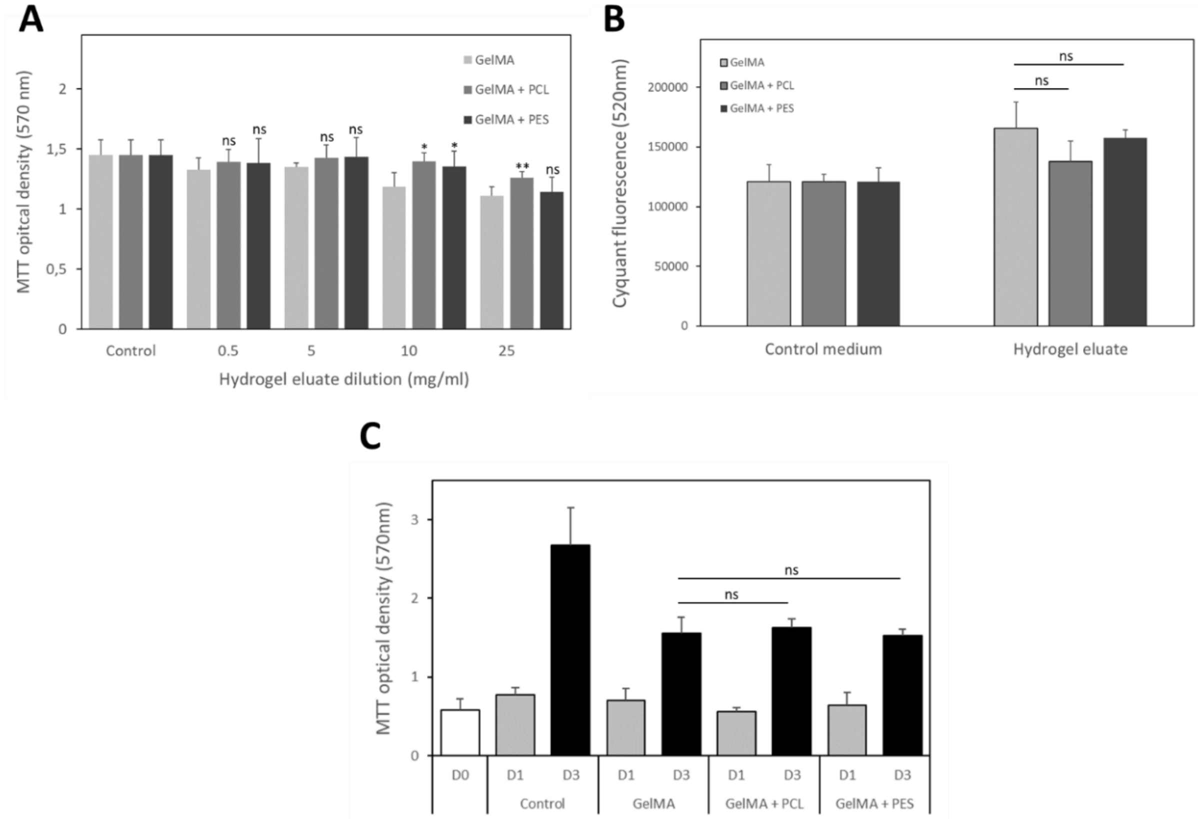

Figure 5. Compatibility of GelMA hydrogels with human keratinocytes. A. Effect of various dilutions of GelMA, GelMA_PCL or GelMA_PES hydrogel eluates on HaCaT cell viability at 24 hours of culture evaluated using the MTT assay. B. Effect of hydrogel eluate on HaCaT cell viability evaluated using the Cyquant assay. C. HaCaT cell proliferation evaluated at day 1 and 3 after seeding evaluated by the MTT assay. Statistical analysis were performed using the Student t-test or the Mann-Whitney test to compare GelMA with or without microspheres.

To determine that human keratinocytes were able to adhere on the different hydrogels, we first compared HaCaT cells viability when seeded either on the three different matrices or directly in the culture plate well. As shown in Figure 6A, the use of the Alamar blue HS assay did not reveal a significant decrease in cell viability when cells were seeded onto the hydrogels. Finally, to validate these results, scanning electron microscopy analysis of HaCaT cells grown onto different hydrogels was performed. As shown in Figure 6B, human keratinocytes adhered and exhibited normal morphology when seeded onto the different GelMA hydrogels. Although HaCaT cells have a very small cytoplasm and do not spread a lot, the highest magnification clearly showed cell surface invaginations and contacts with the different matrices. At the second magnification (scale bar 40 µm), PCL or PES microspheres are present at the surface of the corresponding hydrogels (white arrows). Altogether, these data confirm the *in vitro* cytocompatibility of the materials.

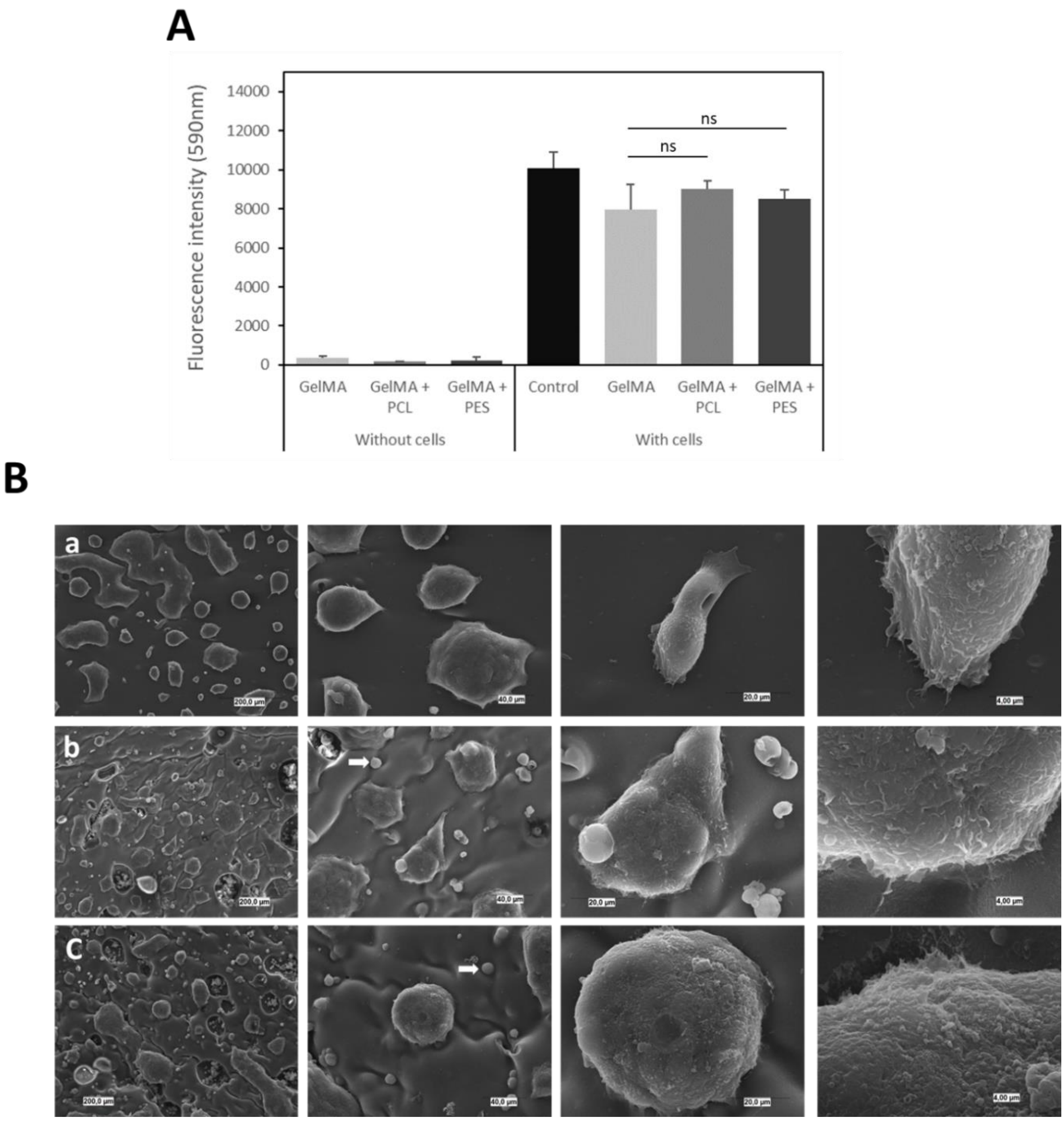

Figure 6. Adhesion and viability of human keratinocytes grown onto the GelMA hydrogels. **A.** Viability of HaCaT cell grown during 16 hours on the matrices. Cell viability was assessed using the Alamar blue assay. The fluorescence intensity corresponding to the same amount of cells seeded in a culture plate well (control) is provided for comparison. The level of fluorescence obtained on hydrogels without cell seeding is also shown. **B.** Scanning electron microscopy images showing HaCaT cells grown on the hydrogels (scale bar of 200, 40, 20 and 4 µm, as indicated). Images show pure GelMA hydrogel (a), with PCL (b) or with PES (c) microspheres. Statistical analysis were performed using the Mann-Whitney test to compare GelMA with or without microspheres.

Swelling of the matrices

Swelling of the drug carrier is one of the mechanisms controlling the rate of the drug release process [51]. In addition, an insightful characterization of the degree of swelling of the matrices makes it possible to assess their suitability as drug delivery systems, as well as to predict their behavior under *in vivo* conditions.

Therefore, in the next stage of the study, the swelling degree of non-modified lyophilized GelMA/gelatin was evaluated as well as the swelling degree of the ones modified with PCL and PES microspheres previously subjected to UV-cross-linking (for 5 min and 10 min). Due to the potential use of such matrices as modified drug release systems, the swelling degree study was conducted for 8 h. Figure 75 shows kinetic swelling curves of the GelMA/gelatin matrices (Tab. 1) examined in PBS buffer.

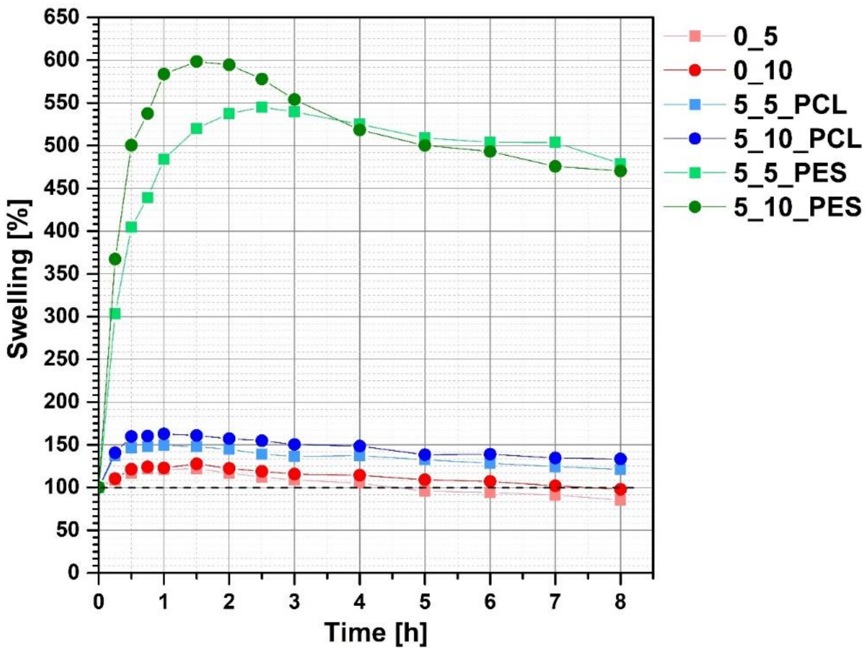

Figure 7. Equilibrium swelling ratio of lyophilized GelMA/gelatin matrices depending on the microsphere content and cross-linking time. In order to facilitate tracking the experimental points, they are connected by line segments from left to right.

As can be seen from Figure 76, 3D bioprinted matrices without microspheres and those containing PCL microspheres reach equilibrium after about 1 h. The maximum hydration is about 125% and 150% for GelMA/gelatin matrices without microspheres and those containing PCL microspheres, respectively. Completely different effects are observed for GelMA/gelatin matrices modified with PES microspheres. They swell much faster reaching a maximum hydration of 550–600% after about 1.5–2 h. Moreover, in the case of this system, a slight loss of weight during the test is also observed. We see the reason for these effects in the completely different morphology (before swelling) of the 3D printed matrices containing PES microspheres

(Fig. 2, image H), which was discussed in the *3D bioprinting feasibility* section. In all likelihood, such a morphology results in easier solvent penetration and thus a very high degree of swelling of the 3D printed matrix modified with PES microspheres. In addition, analysis of Figure 7 shows that the effect of UV-cross-linking time on the swelling of the 3D printed matrices tested is small for all materials tested. It should also be noted that non-cross-linked GelMA/gelatin matrices degraded immediately upon contact with water, confirming the necessity of UV-cross-linking of the matrices using the GelMA-based bioink we developed.

Rhodamine release from GelMA/gelatin matrices

One of the most important conditions that a 3D printed system with a potential use in biomedical engineering field must meet is its proper transport properties. This process should be as controllable as possible – it should run undisturbed (for example, without the burst effect at the beginning) and the appropriate selection of process conditions should lead to release of a defined amount of a substance at a certain rate. Hence, the GelMA/gelatin matrices have been tested in this regard using rhodamine as an active substance marker. The results in the form of release profile plots over the period of 7 hours and a bar graph with its concentration after 24 h of releasing are shown in Figure 8. The curves are divided into three groups differing in colors, red for GelMA/gelatin matrices without microspheres, blue and green for the matrices loaded with PCL or PES microspheres, respectively.

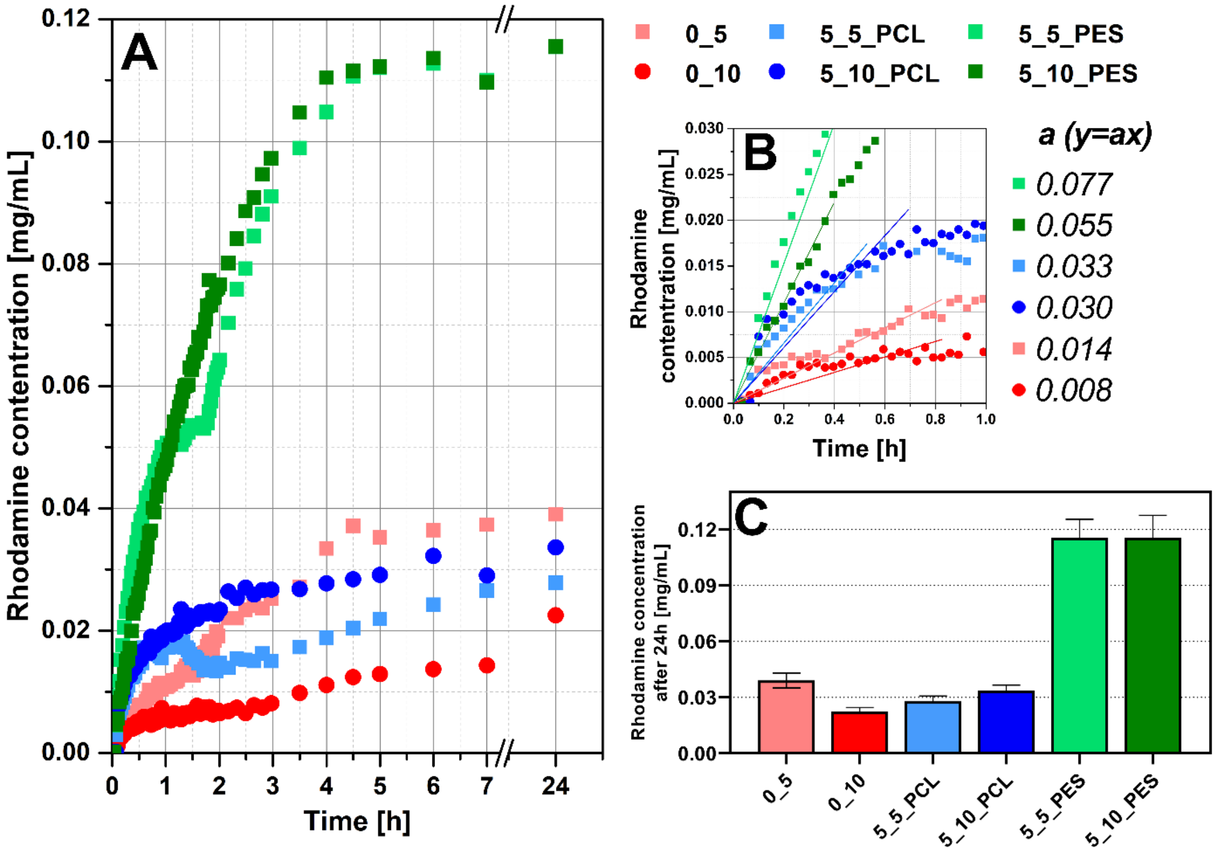

Figure 8. Results of the studies of rhodamine release from GelMA/gelatin matrices depending on microsphere content and UV-cross-linking time. (A) Marker release profiles over the period of 24 hours. (B) Close-up of the first release period (first one hour) with linear model fit (formula $y = ax$), the values of a parameter are given in the list next to the graph. (C) Rhodamine concentration after 24 hours of release from UV-cross-linked GelMA/gelatin matrices with the addition of substance-loaded microspheres depending on the microsphere type and cross-linking time.

No burst effect (referring to very rapid initial increase in the marker concentration above the equilibrium concentration reached later) was observed in any of the examined cases, which is a very desirable property of drug delivery system. The curves describing the release of rhodamine from the matrices (Fig. 8A) are consistent with the curves for the equilibrium swelling ratio (Figure 7). Such a phenomenon was noticed in one of our previous works [23], in which the release of rhodamine from 3D bioprinted gelatin-alginate matrices cross-linked with glutaraldehyde and calcium ions was described. Water is absorbed into the structure of a hydrogel matrix when it is immersed in the solution, dissolving the rhodamine. The marker will not be released into the solution until it has been dissolved in the hydrating water. The continuous release rate results from hydrogel saturation – the release rate is swelling dependent, because only the swollen matrix is permeable to rhodamine. This phenomenon limits the aforementioned burst effect and that the release in the first period follows the zero-order kinetics, so the process can be described mathematically by a linear equation. Such an approach to the problem of release of substances from swelling hydrogels has already been described [23], [52], [53].

Therefore, to determine the substance release rate from the matrices, a linear function was fitted to the points describing the change in rhodamine concentration in the initial period of the experiment (one hour), and its slope coefficient *a* was determined (Fig. 8B). The values of the coefficient of determination R^2 for all fits ranged from 0.9361 to 0.9960, they were therefore very good and the model is suitable for describing the experiment under study. The tested samples form three distinct groups that differ in the rate of rhodamine release. It is the fastest for matrices loaded with PES microspheres, then about two times slower for the ones with PCL microspheres, and the slowest for matrices without microspheres, 5 – 6 times slower than for those PES-loaded. Furthermore, it can be seen that the longer the cross-linking time, the slower the release process in each case.

The use of matrices loaded with PES microspheres clearly increases the amount of rhodamine released after 24 hours compared to the other samples (Fig. 8C). The equilibrium concentration of rhodamine is reached only after 5 hours in this case and it is about 0.11 mg/mL – 3 to 10 times higher than in other cases (matrices with PCL microspheres or no microspheres), where the equilibrium is not reached even after 24 hours.

Some studies on the release of substances from hydrogel matrices modified with microspheres have already been conducted. Fahimipour et al. [26] investigated vascular endothelial growth factor (VEGF) release from biodegradable 3D tricalcium phosphate-based scaffolds containing VEGF-loaded PLGA microspheres. They showed that the release rate in the initial phase from the construct containing microspheres was slower than from the PLGA microspheres. However, they did not eliminate a burst effect by using microspheres in the 3D bioprinted construct, which was ensured by GelMA/gelatin matrices modified with PCL/PES microspheres proposed in presented work. Moreover, Chen et al. [30] were able to demonstrate that the use of gelatin methacryloyl (GelMA)/chitosan microspheres in the 3D bioprinted construct allows prolonged release of nerve growth factor (NGF) from the scaffolds over 9 hours. However, they conducted the study with a less precise method (fluorescence microscopy) than spectrophotometric determination of the substance concentration and made only a few measurements, the first one after 0.5 h. Therefore, it cannot be said whether the burst effect was eliminated in their system. The use of spectrophotometry for determination of rhodamine concentration in our work allowed to define the exact release profile of the substance in the first stage, and these studies clearly showed that the burst effect was eliminated by using microsphere-loaded GelMA/gelatin matrices.

Antibacterial activity

Considering the potential use of microsphere-loaded 3D printed matrices, among others, as dressing materials in the last stage of the study we evaluated their ability to be loaded with an antibiotic in order to acquire antibacterial properties. An agar diffusion inhibition growth assay was performed to characterize the antimicrobial activity of the 3D bioprinted matrices selected for the study. The measurement of the antibacterial activity studies was conducted for four types of 3D printed matrices *i.e.* without ampicillin, with ampicillin, with ampicillin-loaded PCL microspheres and with ampicillin-loaded PES microspheres. The amount of microspheres in the tested matrices was 5 mg/ml of the bioink used in the 3D printing process. Tests were conducted only for materials cross-linked for 10 min with UV. Each sample was deposited on the surface of nutrient agar plate previously inoculated with 1 mL of *E. coli* or *S. aureus* bacteria suspension at a concentration of 10^8 CFU/mL and incubated for 24h. Figure 77. illustrates the results of antibacterial activity tests.

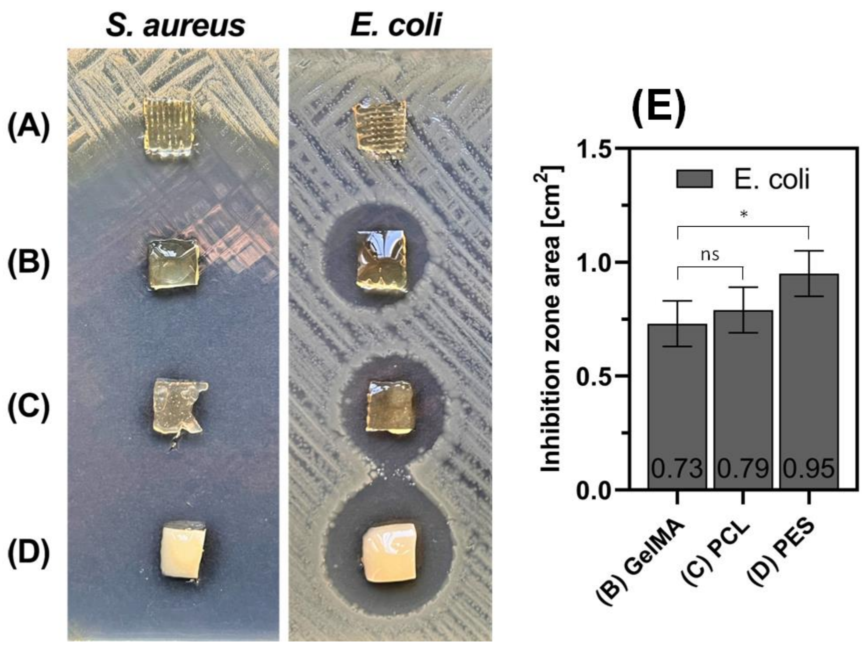

Figure 9. Antibacterial activity of ampicillin-loaded GelMA/gelatin matrices depending on the microsphere content. Nutrient agar plates covered with *S. aureus* and *E. coli* biofilms after 24 h of material treatment. (A) control matrices with no drug. (B) drug-loaded matrices without microspheres. (C – D) matrices with drug-loaded (C) PCL or (D) PES microspheres. (E) A graphical representation in the form of a bar chart illustrating the mean values of inhibition zone areas [cm^2] calculated using Petri dish images obtained from three independent test replicates for *E. coli*. Statistical analysis was performed using ANOVA followed by a post-hoc Tukey HSD test.

The study showed that all the drug-containing 3D printed matrices tested had antimicrobial activity, most potent against *S. aureus* bacteria (overlapping inhibition zones making them impossible to measure). A comparable phenomenon of varying antibiotic effectiveness depending on the bacterial type has been previously documented [23]. For *E. coli* bacteria matrices modified with PES microspheres show slightly higher antibacterial activity (as evidenced by a bit larger zone of growth inhibition – clear zones) than those modified with PCL microspheres which is confirmed by calculated areas of inhibition zones (Fig. 9E). These results correspond very well with the results of rhodamine release studies described in an earlier section (Fig. 8C). 3D printed matrices without drug and without microspheres showed no antibacterial activity, and the clear zone observed for sample A is the result of the very strong effect of the drug present in sample B against *S. aureus* bacteria (Fig. 9). The remarkable difference in the size of the inhibited growth zones for *S. aureus* compared to *E. coli* should be noted. The observed antibacterial activity of the matrices against the bacteria provides evidence that the drug integrity remained intact during both microsphere preparation and 3D bioprinting processes. As a result, the suggested 3D bioprinted matrices could potentially be used as controlled drug delivery systems.

CONCLUSIONS

A new bioink containing gelatin methacrylate, gelatin and LAP photoinitiator modified by the addition of either PCL or PES microspheres is a good material for application in 3D bioprinting using the extrusion technique. 3D bioprinted model can be cross-linked using UV light, creating a water-insoluble compact structure. The cross-linking time has almost no effect on the properties of the printed matrices. However, the obtained systems essentially differ depending on whether and what kind of microspheres was dispersed in the bioink.

The addition of PES microspheres to a bioink used for 3D bioprinting leads to a different structure of the printed matrix (than the one without microspheres or PCL-modified one) due to changes in thermal properties. The PES-modified matrices have a higher swelling degree. They are characterized by four times higher drug capacity than other tested systems and faster drug release with no burst effect. The other two systems (without microspheres and with PCL ones) are characterized by a lower drug capacity, nevertheless, the time of its release is longer which is beneficial for long-term therapies. Furthermore, the matrices with microspheres have higher degradation temperatures, which is beneficial in terms of the potential use of bioprinted hydrogels in biomedical engineering due to the autoclave sterilization process. All tested types of matrices are non-cytotoxic and can be loaded with antibiotic to acquire antibacterial properties against both Gram-positive and Gram-negative bacteria.

The new bioinks modified with microspheres presented in the work are a very good starting point for the design of various constructs with potential biomedical application, for example as controlled drug delivery systems or wound dressings.

ACKNOWLEDGEMENTS

The authors are grateful to Chantal Cazevieille (CoMET, Institut des Neurosciences Montpellier) for her technical assistance and for the interpretation of electron microscopy data. This project was supported by European Social Fund [POWR.03.02.00-00-1028/17-00] as part of the POWER Och!Dok program. AM would like to thank Campus France for the funding through a French Government Scholarship. Authors acknowledge the financial support of project H2020-MSCA-RISE-2017, "Novel 1D photonic metal oxide nanostructures for early stage cancer detection" (Project number: 778157). The authors are grateful to Chantal Cazevieille (CoMET, Institut des Neurosciences Montpellier) for her technical assistance and for the interpretation of electron microscopy data.

REFERENCES

[1] S. Beg, W. H. Almalki, A. Malik, M. Farhan, M. Aatif, Z. Rahman, N. K. Alruwaili, M. Alrobaian, M. Tarique, M. Rahman, 3D printing for drug delivery and biomedical applications, *Drug Discov. Today*, 2020, **25**, 1668–1681.

[2] A. C. Daly, M. E. Prendergast, A. J. Hughes, J. A. Burdick, Bioprinting for the Biologist, *Cell*, 2021, **184**, 18–32.

[3] B. Tan, S. Gan, X. Wang, W. Liu, X. Li, Applications of 3D bioprinting in tissue engineering: advantages, deficiencies, improvements, and future perspectives, *J. Mater. Chem. B*, 2021, **9**, 5385–5413.

[4] G. Gao, M. Ahn, W. W. Cho, B. S. Kim, D. W. Cho, 3D printing of pharmaceutical application: Drug screening and drug delivery, *Pharmaceutics*, 2021, **13**, 1373, DOI: 10.3390/pharmaceutics13091373.

[5] A. P. Tiwari, N. D. Thorat, S. Pricl, R. M. Patil, S. Rohiwal, H. Townley, Bioink: a 3D-bioprinting tool for anticancer drug discovery and cancer management, *Drug Discov. Today*, 2021, **26**, 1574–1590.

[6] C. Karavasili, G. K. Eleftheriadis, C. Gioumouxouzis, E. G. Andriotis, D. G. Fatouros, Mucosal drug delivery and 3D printing technologies: A focus on special patient populations, *Adv. Drug Deliv. Rev.*, 2021, **176**, 113858, DOI: 10.1016/j.addr.2021.113858.

[7] P. Jain, H. Kathuria, N. Dubey, Advances in 3D bioprinting of tissues/organs for regenerative medicine and in-vitro models, *Biomaterials*, 2022, **287**, 121639, DOI: 10.1016/j.biomaterials.2022.121639.

[8] G. Saini, N. Segaran, J. L. Mayer, A. Saini, H. Albadawi, R. Oklu, Applications of 3d bioprinting in tissue engineering and regenerative medicine, *J. Clin. Med.*, 2021, **10**, 4966, DOI: 10.3390/jcm10214966.
[9] Z. Wang, W. Kapadia, C. Li, F. Lin, R.F. Pereira, P.L. Granja, B. Sarmento, W. Cui, Tissue-specific engineering: 3D bioprinting in regenerative medicine, *J. Control. Release*, 2021, **329**, 237–256.
[10] Y. W. Ding, X. W. Zhang, C. H. Mi, X. Y. Qi, J. Zhou, D. X. Wei, Recent advances in hyaluronic acid-based hydrogels for 3D bioprinting in tissue engineering applications, *Smart Materials in Medicine*, 2023, **4**, 59–68.
[11] D. Williams, P. Thayer, H. Martinez, E. Gatenholm, A. Khademhosseini, A perspective on the physical, mechanical and biological specifications of bioinks and the development of functional tissues in 3D bioprinting, *Bioprinting*, 2018, **9**, 19–36.
[12] L. Valot, J. Martinez, A. Mehdi, G. Subra, Chemical insights into bioinks for 3D printing Chemical insights in bioinks for 3D printing, *R. Soc. Chem.*, 2019, **48**, 4049–4086.
[13] J. Gopinathan, I. Noh, Recent trends in bioinks for 3D printing, *Biomater. Res.*, 2018, **22**, DOI: 10.1186/s40824-018-0122-1.
[14] S. Vanaei, M. S. Parizi, F. Salemizadehparizi, H. R. Vanaei, An Overview on Materials and Techniques in 3D Bioprinting Toward Biomedical Application, *Engineered Regeneration*, 2021, **2**, 1–18.
[15] R. Staros, A. Michalak, K. Rusinek, K. Mucha, Z. Pojda, R. Zagożdżon, Perspectives for 3D-Bioprinting in Modeling of Tumor Immune Evasion, *Cancers*, 2022, **14**, 3126, DOI: 10.3390/cancers14133126.
[16] A. B. Bello, D. Kim, D. Kim, H. Park, S. H. Lee, Engineering and functionalization of gelatin biomaterials: From cell culture to medical applications, *Tissue Eng. Part B Rev.*, 2020, **26**, 164–180.
[17] G. Ying, N. Jiang, C. Yu, Y. S. Zhang, Three-dimensional bioprinting of gelatin methacryloyl (GelMA), *Bio-Des. Manuf.*, 2018, **1**, 215–224.
[18] R. L. Alexa, H. Iovu, J. Ghitman, A. Serafim, C. Stavarache, M.-M. Marin, R. Ianchis, 3D-printed gelatin methacryloyl-based scaffolds with potential application in tissue engineering, *Polymers*, 2021, **13**, 727, DOI: 10.3390/polym13050727.
[19] K. Yue, G. Trujillo-de Santiago, M. Alvarez, A. Tamayol, N. Annabi, A. Khademhosseini, Synthesis, properties, and biomedical applications of gelatin methacryloyl (GelMA) hydrogels, *Biomaterials*, 2015, **73**, 254-271.
[20] Y. Piao, H. You, T. Xu, H.-P. Bei, I. Z. Piwko, Y. Y. Kwan, X. Zhao, Biomedical applications of gelatin methacryloyl hydrogels, *Engineered Regeneration*, 2021, **2**, 47–56.
[21] M. Lengyel, N. Kállai-Szabó, V. Antal, A. J. Laki, I. Antal, Microparticles, microspheres, and microcapsules for advanced drug delivery, *Sci. Pharm.*, 2019, **87**, 20, DOI: 10.3390/scipharm87030020.
[22] A. N. Yawalkar, M. A. Pawar, P. R. Vavia, Microspheres for targeted drug delivery - A review on recent applications, *J. Drug Deliv. Sci. Technol.*, 2022, **75**, 103659, DOI: 10.1016/j.jddst.2022.103659.
[23] A. Mirek, H. Belaid, F. Barranger, M. Grzeczkowicz, Y. Bouden, V. Cavaillès, D. Lewińska, M. Bechelany, Development of a new 3D bioprinted antibiotic delivery system based on a cross-linked gelatin-alginate hydrogel, *J. Mater. Chem. B,* 2022, **10**, 8862–8874.
[24] Y. J. Tan, X. Tan, W. Y. Yeong, S. B. Tor, Hybrid microscaffold-based 3D bioprinting of multi-cellular constructs with high compressive strength: A new biofabrication strategy, *Sci. Rep.*, 2016, **6**, DOI: 10.1038/srep39140.
[25] L. K. Narayanan, P. Huebner, M. B. Fisher, J. T. Spang, B. Starly, R. A. Shirwaiker, 3D-Bioprinting of Polylactic Acid (PLA) Nanofiber-Alginate Hydrogel Bioink Containing Human Adipose-Derived Stem Cells, *ACS Biomater. Sci. Eng.*, 2016, **2**, 1732–1742.

[26] F. Fahimipour, M. Rasoulianboroujeni, E. Dashtimoghadam, K. Khoshroo, M. Tahriri, F. Bastami, D. Lobner, L. Tayebi, 3D printed TCP-based scaffold incorporating VEGF-loaded PLGA microspheres for craniofacial tissue engineering, *Dent. Mater.*, 2017, **33**, 1205–1216.
[27] H. Xu, J. Casillas, C. Xu, Effects of printing conditions on cell distribution within microspheres during inkjet-based bioprinting, *AIP Adv*, 2019, **9**, 095055, DOI: 10.1063/1.5116371.
[28] D. L. Johnson, R. M. Ziemba, J. H. Shebesta, J. C. Lipscomb, Y. Wang, Y. Wu, K. D. O'Connell, M. G. Kaltchev, A. van Groningen, J. Chen, Design of pectin-based bioink containing bioactive agent-loaded microspheres for bioprinting, *Biomed. Phys. Eng. Express*, 2019, **5**, DOI: 10.1088/2057-1976/ab4dbc.
[29] B. Mirani, E. Pagan, S. Shojaei, J. Duchscherer, B. D. Toyota, S. Ghavami, M. Akbari, 3D bioprinted hydrogel mesh loaded with all-trans retinoic acid for treatment of glioblastoma, *Eur. J. Pharmacol.*, 2019, **854**, 201–212.
[30] J. Chen, D. Huang, L. Wang, J. Hou, H. Zhang, Y. Li, S. Zhong, Y. Wang, Y. Wu, W. Huang, 3D bioprinted multiscale composite scaffolds based on gelatin methacryloyl (GelMA)/chitosan microspheres as a modular bioink for enhancing 3D neurite outgrowth and elongation, *J. Colloid Interface Sci.*, 2020, **574**, 162–173.
[31] R. Sharma, I. P. M. Smits, L. de La Vega, C. Lee, S. M. Willerth, 3D Bioprinting Pluripotent Stem Cell Derived Neural Tissues Using a Novel Fibrin Bioink Containing Drug Releasing Microspheres, *Front. Bioeng. Biotechnol.*, 2020, **8**, DOI: 10.3389/fbioe.2020.00057.
[32] R. Sharma, R. Kirsch, K. P. Valente, M. R. Perez, S. M. Willerth, Physical and mechanical characterization of fibrin-based bioprinted constructs containing drug-releasing microspheres for neural tissue engineering applications, *Processes*, 2021, **9**, 1205, DOI: 10.3390/pr9071205.
[33] R. Sharma, C. Benwood, S. M. Willerth, Drug-releasing Microspheres for Stem Cell Differentiation, *Curr. Protoc.*, 2021, **1**, DOI: 10.1002/cpz1.331.
[34] M. Kanungo, Y. Wang, N. Hutchinson, E. Kroll, A. DeBruine, S. Kumpaty, L. Ren, Y. Wu, X. Hua, W. Zhang, Development of gelatin-coated microspheres for novel bioink design, *Polymers*, 2021, **13**, 3339, DOI: 10.3390/polym13193339.
[35] L. de la Vega, L. Abelseth, R. Sharma, J. Triviño-Paredes, M. Restan, S. M. Willerth, 3D Bioprinting Human-Induced Pluripotent Stem Cells and Drug-Releasing Microspheres to Produce Responsive Neural Tissues, *Adv. Nanobiomed. Res.*, 2021, **1**, 2000077, DOI: 10.1002/anbr.202000077.
[36] M. Bonany, L. del-Mazo-Barbara, M. Espanol, M.-P. Ginebra, Microsphere incorporation as a strategy to tune the biological performance of bioinks, *J. Tissue Eng.*, 2022, **13**, 204173142211198, DOI: 10.1177/20417314221119895.
[37] A. Mirek, M. Grzeczkowicz, C. Lamboux, S. Sayegh, M. Bechelany, D. Lewińska, Formation of disaggregated polymer microspheres by a novel method combining pulsed voltage electrospray and wet phase inversion techniques, *Colloids Surf. A: Physicochem. Eng. Asp.*, 2022, **648**, 129246, DOI: 10.1016/j.colsurfa.2022.129246.
[38] J. Yin, M. Yan, Y. Wang, J. Fu, H. Suo, 3D Bioprinting of Low-Concentration Cell-Laden Gelatin Methacrylate (GelMA) Bioinks with a Two-Step Cross-linking Strategy, *ACS Appl. Mater. Interfaces*, 2018, **10**, 6849–6857.
[39] A. I. van den Bulcke, B. Bogdanov, N. de Rooze, E. H. Schacht, M. Cornelissen, H. Berghmans, Structural and rheological properties of methacrylamide modified gelatin hydrogels, *Biomacromolecules*, 2000, **1**, 31–38.
[40] Allevi, Inc., Allevi Protocols: Cell-Bioink Mixing: Syringe Coupler Method, Allevi, https://www.allevi3d.com/cell-bioink-mixing-syringe-coupler-method/, (accessed 16 August 2022).
[41] O. Jeon, Y. B. Lee, S. J. Lee, N. Guliyeva, J. Lee i E. Alsberg, Stem cell-laden hydrogel bioink for generation of high resolution and fidelity engineered tissues with complex geometries, *Bioactive Materials*, 2022, **15**, 185-193.

[42] M. Grzeczkowicz, D. Lewińska, A method for investigating transport properties of partly biodegradable spherical membranes using vitamin B12 as the marker, *Desalin. Water Treat.*, 2018, **128**, 170–178.
[43] C. Funaki, S. Yamamoto, H. Hoshina, Y. Ozaki, H. Sato, Three different kinds of weak C-H···O=C inter- and intramolecular interactions in poly(ε-caprolactone) studied by using terahertz spectroscopy, infrared spectroscopy and quantum chemical calculations, *Polymer,* 2018, **137**, 245–254.
[44] H. Lu, H. Shinzawa, S. G. Kazarian, Intermolecular Interactions in the Polymer Blends Under High-Pressure CO2 Studied Using Two-Dimensional Correlation Analysis and Two-Dimensional Disrelation Mapping, *Appl. Spectrosc.*, 2021, **75**, 250–258.
[45] H. Hatakeyama A, T. Hatakeyama, Interaction between water and hydrophilic polymers, *Thermochim. Acta*, 1998, **308**, 3–22.
[46] M. Rusu, M. Ursu, D. Rusu, Poly(vinyl chloride) and Poly(e-caprolactone) Blends for Medical Use, *J. Thermoplas. Compos. Mater.*, 2006, **19**, 173–190.
[47] T. Tavangar, A. Hemmati, M. Karimi, F. Zokaee Ashtiani, Layer-by-layer assembly of graphene oxide (GO) on sulfonated polyethersulfone (SPES) substrate for effective dye removal, *Polymer Bulletin*, 2019, **76**, 35–52.
[48] M. U. Joardder, M. Mourshed, M. Hasan Masud, Bound water measurement techniques, in: *State of Bound Water: Measurement and Significance in Food Processing*, Springer International Publishing, NYC, 2019, 47–82.
[49] H. Yoshida, T. Hatakeyama, H. Hatakeyama, *Effect of water on the main chain motion of polysaccharide hydrogels*, W.G. Glasser, H. Hatakeyama (Eds.), Viscoelasticity of biomaterials. ACS symposium series, **489**, ACS, Washington, 1992, 218–230.
[50] S. Ramesh, M. Ramalingam, Aqueous-mediated synthesis and characterization of gelatin methacryloyl for biomedical applications, *Biointerface Res. App.l Chem.*, 2022, **12**, 6269–6279.
[51] M. Rizwan, R. Yahya, A. Hassan, M. Yar, A. D. Azzahari, V. Selvanathan, F. Sonsudin, C. N. Abouloula, pH sensitive hydrogels in drug delivery: Brief history, properties, swelling, and release mechanism, material selection and applications, *Polymers*, 2017, **9**, 137, DOI: 10.3390/polym9040137.
[52] M. L. Laracuente, M. H. Yu, K. J. McHugh, Zero-order drug delivery: State of the art and future prospects, *J. Control. Release*, 2020, **327**, 834–856.
[53] M. L. Bruschi, Mathematical models of drug release, in: *Strategies to Modify the Drug Release from Pharmaceutical Systems*, Woodhead Publishing: Cambridge, UK, 2015, 63–86.